Coupled dynamics of voltage and calcium in paced cardiac cells

Yohannes Shiferaw,[1,2] Daisuke Sato,[1] and Alain Karma[1]
[1]*Department of Physics and Center for Interdisciplinary Research on Complex Systems, Northeastern University, Boston, Massachusetts 02115, USA*
[2]*Department of Medicine and Cardiology, University of California, Los Angeles, California 90095-1679, USA*
(Received 10 May 2004; published 8 February 2005)

We investigate numerically and analytically the coupled dynamics of transmembrane voltage and intracellular calcium cycling in paced cardiac cells using a detailed physiological model, and its reduction to a three-dimensional discrete map. The results provide a theoretical framework to interpret various experimentally observed modes of instability ranging from electromechanically concordant and discordant alternans to quasiperiodic oscillations of voltage and calcium.

DOI: 10.1103/PhysRevE.71.021903 PACS number(s): 87.19.Hh, 82.40.Bj, 05.45.Tp

I. INTRODUCTION

Over the last decade, there has been a growing recognition that dynamic instability of the cardiac action potential can play a crucial role in the initiation of life-threatening arrhythmias [1–6]. Most studies to date have focused on the dynamics of the transmembrane voltage governed by the standard equation

$$\dot{V} = -(I_{\rm ion} + I_{\rm ext})/C_m, \tag{1}$$

where C_m is the membrane capacitance, $I_{\rm ion}$ is the total membrane current, which is the sum of the individual currents for Na^+, K^+, and Ca^+ ions depicted schematically in Fig. 1, and $I_{\rm ext}$ is a current stimulus applied at equally spaced time intervals T. A widely used approach to model the nonlinear dynamics of voltage is the one-dimensional discrete map $A_{n+1}=f(T-A_n)$ which relates the action potential duration (APD) at two subsequent beats via the restitution curve, $A_{n+1}=f(D_n)$, where D_n is the interval between the end of the previous action potential and the next [1–6]. The periodic fixed point of this map corresponding to the stable 1:1 rhythm undergoes a period-doubling instability to alternans, a sequence of long (L) and short (S) (LSLS…) APD, when the slope of the restitution curve is >1.

Even though this map has been successful to model the unstable dynamics of voltage in some ionic models [3] and experiments [4], its predictions are inconsistent with a wide range of observations [5–8]. For example, Hall *et al.* [5] found that alternans can be absent even when the slope of the experimentally measured restitution curve is significantly larger than one, and conversely alternans are observed under ischemic conditions in which the restitution curve is flat [8]. Furthermore, recent experimental [7,9,10] and theoretical studies [11] suggest that alternans may result from an instability of intracellular calcium cycling. This result clearly indicates that the dynamical behavior of a cardiac cell is governed by nonlinear processes that are not taken into account by the restitution relationship.

In this article we explore the coupled nonlinear dynamics of voltage and calcium cycling in paced cardiac cells using a physiologically based ionic model. We demonstrate that a paced cell can be unstable to three distinct dynamical modes: concordant alternans with a long/short APD corresponding to a large/small calcium transient on alternate beats, discordant alternans with a long/short APD corresponding to a small/large calcium transient, and modulated voltage/calcium alternans with amplitudes that vary sinusoidally in time. The physiological conditions which favor a given dynamical behavior are explained. Finally, we interpret the model results in terms of a three variable iterated map which describes the beat-to-beat dynamics of calcium and voltage.

II. IONIC MODEL

A. Calcium cycling

To describe the electrophysiology of a cardiac myocyte we integrate a recently developed model of calcium (Ca^{2+}) cycling [11], with an established ionic model due to Fox *et al.* [12] that is based on the Luo-Rudy currents [13]. The ionic currents, along with elements of the calcium cycling system, are illustrated in Fig. 1. The movement of calcium inside the cell is described by

$$\dot{c}_s = \frac{\beta_s v_i}{v_s}\left[I_{\rm rel} - \frac{c_s - c_i}{\tau_s} - I_{\rm Ca} + I_{\rm NaCa} \right] - \beta_s I_{\rm tr}^s, \tag{2}$$

$$\dot{c}_i = \beta_i \left[\frac{c_i - c_s}{\tau_s} - I_{\rm up} - I_{\rm tr}^i \right], \tag{3}$$

$$\dot{c}_j = -I_{\rm rel} + I_{\rm up}, \tag{4}$$

$$\dot{c}_j' = \frac{c_j - c_j'}{\tau_a}, \tag{5}$$

$$\dot{I}_{\rm rel} = g I_{\rm Ca} Q(c_j') - \frac{I_{\rm rel}}{\tau_r}, \tag{6}$$

where c_s, c_i, and c_j are the concentrations of free calcium in a thin layer just below the cell membrane (submembrane space), in the bulk myoplasm, and the sarcoplasmic recticulum (SR), with volumes v_s, v_i, and $v_{\rm sr}$, respectively, where the SR volume includes both the junctional SR (JSR) and the

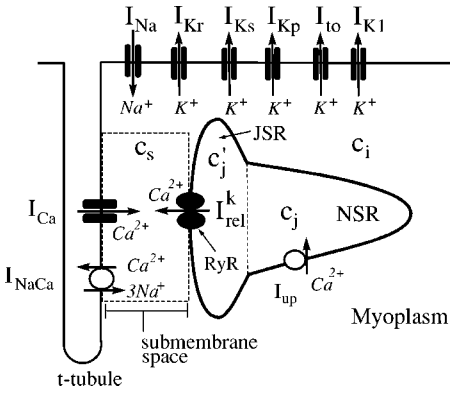

FIG. 1. Illustration of currents that control the dynamics of voltage and intracellular calcium cycling.

network SR (NSR); c_j' is the average JSR concentration in the whole cell as defined in Ref. [11]. The concentrations c_s and c_i are in units of μM, whereas c_j and c_j' are in units of $\mu M v_{sr}/v_i$. All calcium fluxes are divided by v_i and have units of $\mu M/s$. Instantaneous buffering of calcium to SR and calmodulin sites in v_i and v_s is accounted for by the functions $\beta_s \equiv \beta(c_s)$ and $\beta_i \equiv \beta(c_i)$, and the currents $I_{tr}^{s,i}$ describe time-dependent buffering to troponin C [11].

Calcium release from the SR is triggered by calcium entry into the cell via calcium-induced calcium release (CICR) [14]. Release occurs at a very large number of junctions where several *L*-type calcium channels (I_{Ca}) and a few release channels (ryanodine receptors; RyRs) face each other in close proximity. Only one of these junctions is shown in Fig. 1 for clarity. The total release current for the whole cell is the sum $I_{rel}=\Sigma_{k=1}^{N(t)} I_{rel}^k$, of local currents I_{rel}^k at each junction where release channels are activated. The number of sparks $N(t)$ varies in time since sparks are recruited stochastically and extinguish. The spatially localized nature of release is described by the dynamical equation for the release current [Eq. (6)], which captures phenomenologically three key experimental observations: (i) sparks are recruited at a rate proportional to the whole cell I_{Ca}, or $\dot{N} \sim I_{Ca}$ [16], which insures that calcium release is graded with respect to calcium entry [15,17], (ii) the spark lifetime τ_r is approximately constant, and (iii) the amount of calcium released increases with SR concentration (SR load) [18].

B. Instability mechanisms

Calcium alternans, a period-doubling sequence of large (*l*) and small (*s*) calcium transient (*lsls*… peak c_i), can occur independently of voltage alternans in experiments with a single cell paced with a periodic voltage wave form [9]. Both theoretical analyses [11,19] and recent experiments [10] support that a steep dependence of release on SR load is the underlying mechanism of these alternans. The sensitivity of release to SR load is controlled in the model by the slope of the function $Q(c_j')$ at high load

$$u \equiv dQ/dc_j'. \tag{7}$$

For a large enough slope, the model produces calcium alternans when paced with a periodic voltage wave form [11] as in the experiments of Ref. [9].

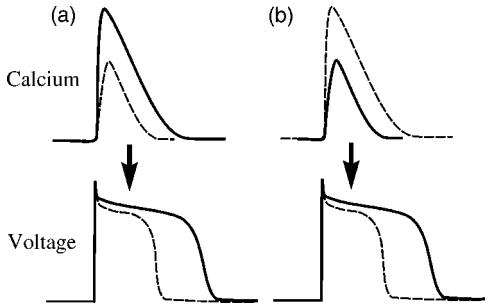

FIG. 2. Illustration of the effect of an increase in the magnitude of the calcium transient, which can prolong or shorten the APD for (a) positive and (b) negative coupling, respectively. The sign of the coupling depends on the relative contributions of I_{Ca} and I_{NaCa} to the APD. The solid or dashed lines correspond to the same beat.

Steep APD restitution in the absence of calcium alternans can also induce APD alternans. This steepness is especially sensitive to the recovery from inactivation of the calcium current [12,13]

$$I_{Ca} = d \cdot f \cdot f_{Ca} \cdot i_{Ca}, \tag{8}$$

where i_{Ca} is the single channel current and $d(f)$ is a fast (slow) voltage-dependent activation (inactivation) gate. For the intermediate range of pacing rates studied in the present work, increasing the time constant τ_f of the f gate in the equation $\dot{f}=[f_\infty(V)-f]/\tau_f$ steepens APD restitution and promotes voltage alternans.

C. Voltage-calcium coupling

The mutual influence of voltage and calcium during the action potential is controlled by the membrane currents that depend on intracellular calcium concentration. These include I_{Ca} and the sodium-calcium exchanger I_{NaCa}. A larger calcium transient following a larger release enhances inactivation of I_{Ca} via the calcium-dependent gate f_{Ca}, and hence shortens the APD, but increases the chemical driving force for calcium extrusion from the cell via the exchanger. Since three Na^+ ions enter the cell for every Ca^{2+} ion extruded, this increase in driving force increases the inward membrane current which prolongs the APD. Therefore, depending on the relative contributions of I_{Ca} and I_{NaCa}, increasing the magnitude of the calcium transient can either prolong (positive coupling) or shorten (negative coupling) the APD, as illustrated in Fig. 2. The sign of this coupling can be changed in the model by varying the exponent γ in the phenomenological expression

$$f_{Ca}^{\infty} = \frac{1}{1+(c_s/\tilde{c}_s)^{\gamma}} \tag{9}$$

for the steady-state value of f_{Ca}, where the constant $\tilde{c}_s$ sets the concentration range for inactivation. Increasing γ enhances calcium-dependent inactivation of I_{Ca} and tends to make the coupling negative.

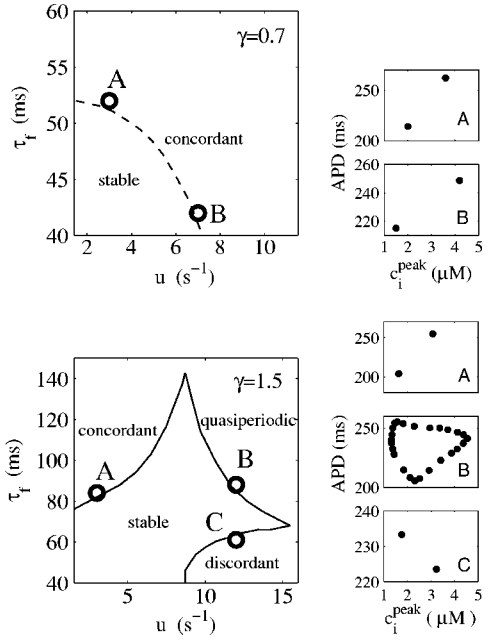

FIG. 3. Stability boundaries in the ionic model for positive (dashed line; $\gamma=0.7$) and negative (solid line; $\gamma=1.5$) coupling. $T=300$ ms. Examples of steady-state dynamics close to the stability boundaries are illustrated by plots of peak calcium concentration (c_i^{peak}) vs APD for a few labeled points. Higher order periodicities and irregular dynamics are observed further away from these boundaries.

III. NUMERICAL RESULTS

The dynamics of the system was studied numerically as a function of the two instability parameters u and τ_f which promote calcium and voltage alternans, respectively, and for two values of γ that were found to yield a positive ($\gamma=0.7$) and a negative ($\gamma=1.5$) coupling between voltage and calcium. All the other parameters are the same as in Refs. [11,12]. We study the stability of the periodic fixed by computing the steady-state APD, and the corresponding peak calcium transient (c_i^{peak}). The APD is computed by measuring the time interval to 80% repolarization. In Fig. 3 we plot the stability boundaries as a function of the model parameters at a fixed pacing rate of $T=300$ ms.

The results plotted in Fig. 3 highlight the crucial role of the coupling between voltage and calcium in the dynamics. For positive coupling, the instability of the 1:1 periodic state always occurs through a period-doubling bifurcation to electromechanically concordant alternans with the long (short) APD corresponding to a large (small) calcium transient, independently of whether voltage or calcium is the dominant instability mechanism. In contrast, for negative coupling, three distinct modes of instability are found that correspond to: (i) concordant alternans, as for positive coupling, but only when the instability is dominated by voltage (large τ_f and small u), (ii) electromechanically discordant alternans with the long (short) APD corresponding to a small (large) calcium transient when the instability is dominated by calcium (small τ_f and large u), and (iii) quasiperiodic oscillations of APD and calcium transient amplitude with a phase and a Hopf frequency that vary with τ_f and u for the in between case where the instability is driven by both voltage and calcium. Both electromechanically concordant and discordant alternans have been widely observed experimentally under various conditions [20]. In addition, there is experimental evidence for quasiperiodicity in recordings of voltage [21] and, more recently, calcium [22].

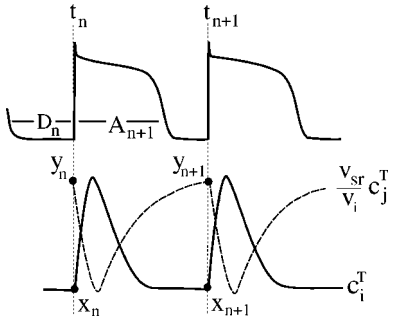

FIG. 4. Definition of map variables.

IV. ITERATED MAP ANALYSIS

A. Iterated map of voltage-calcium dynamics

The numerical findings in the previous section were found to apply at a wide range of pacing intervals T. To interpret our results, and investigate the generality of the findings, we extend the two-dimensional (2D) iterated map developed in Ref. [11] for calcium cycling when the cell is paced with a fixed periodic voltage wave form, to the present case where the voltage is unclamped. To a good approximation, $c_s \approx c_i$ and $c_j' \approx c_j$ preceding a stimulus [11], such that we only need to track beat-to-beat changes of c_i and c_j. Furthermore, we assume for simplicity that buffering of calcium is instantaneous such that there exists a unique nonlinear relationship between the concentration of free calcium $c_i(c_j)$ and total calcium (free plus bound) $c_i^T(c_j^T)$. The basic variables of the map (Fig. 4) are then c_i^T and c_j^T at time $t_n=nT$ of the nth+1 stimulus, defined by $x_n \equiv c_i^T(t_n)$ and $y_n \equiv (v_{\text{sr}}/v_i)c_j^T(t_n)$ where both x_n and y_n are in units of μM, and the APD corresponding to this stimulus, A_{n+1}.

The map is obtained by extending the restitution map to include the effect of calcium on the APD and by integrating the calcium flux equations

$$\dot{c}_i^T = I_{\text{rel}} - I_{\text{up}} - I_{\text{Ca}} + I_{\text{NaCa}}, \tag{10}$$

$$\dot{c}_j^T = (v_i/v_{\text{sr}})(-I_{\text{rel}} + I_{\text{up}}), \tag{11}$$

from time t_n to time t_{n+1}. This yields

$$A_{n+1} = F(D_n, x_n, y_n), \tag{12}$$

$$x_{n+1} = x_n + R_n - U_n + \Delta_n, \tag{13}$$

$$y_{n+1} = y_n - R_n + U_n, \tag{14}$$

respectively, where R_n, U_n, and Δ_n are the integrals of I_{rel}, I_{up}, and $-I_{\text{Ca}}+I_{\text{NaCa}}$ over the time interval $[t_n, t_{n+1}]$, re-

spectively, and are functions of (D_n, x_n, y_n) for a fixed pacing period; $v_i R_n$ and $v_i U_n$ are the total amount of calcium released from and pumped into the SR over one beat, respectively, and $v_i \Delta_n$ is the net total calcium entry into the cell over one beat which can be positive (negative) if the exchanger extrudes more (less) calcium from the cell than I_{Ca} brings into the cell.

B. Stability analysis

To make contact with the numerical stability boundaries in Fig. 3, we study the stability of the fixed point of the iterated map. The fixed point will be denoted by (A^*, x^*, y^*). To begin, we exploit the fact that the total amount of calcium inside the cell is approximately constant during steady-state pacing. Hence, we can approximate the three-dimensional (3D) map [Eqs. (12)–(14)] by a 2D map by assuming that $z_n \approx z^*$, where $v_i z_n \equiv v_i(x_n + y_n)$ is the total calcium in the cell at time t_n. This 2D map is given by Eqs. (12) and (13) with $D_n = T - A_n$, $\Delta_n = 0$, and $y_n = z^* - x_n$. A linear stability analysis of this 2D map yields the eigenvalues

$$\lambda_{\pm} = \frac{1}{2}\left[-\lambda_v - \lambda_c \pm \sqrt{(\lambda_c - \lambda_v)^2 + 4C}\right], \tag{15}$$

where we have defined the quantities

$$\lambda_v = \frac{\partial F}{\partial D_n}, \tag{16}$$

$$\lambda_c = -1 - \frac{\partial (R_n - U_n)}{\partial x_n} + \frac{\partial (R_n - U_n)}{\partial y_n}, \tag{17}$$

$$C = \frac{\partial (R_n - U_n)}{\partial D_n}\left(\frac{\partial F}{\partial y_n} - \frac{\partial F}{\partial x_n}\right), \tag{18}$$

which are evaluated at the fixed point of the map. Here, λ_v and λ_c govern the degree of instability of the voltage and calcium systems, respectively, while C determines the sign of the coupling between the two systems. Making APD restitution $(\partial F / \partial D_n)$ or the relationship between release and SR load $(\partial R_n / \partial y_n)$ steeper by increasing τ_f and u in the ionic model is equivalent to increasing λ_v and λ_c, respectively. Graded release implies that $\partial (R_n - U_n)/\partial D_n$ is positive for high pacing rates where I_{Ca} depends on D_n, such that the sign of C is governed by $\partial F/\partial y_n - \partial F/\partial x_n$ where the latter reflects the effect of the magnitude of the calcium transient on APD via I_{Ca} and I_{NaCa} (Fig. 2). The periodic fixed point undergoes a period-doubling bifurcation when $|\lambda_-| = 1$ and a Hopf bifurcation for $(\lambda_v - \lambda_c)^2 + 4C < 0$ when the pair of complex eigenvalues $\lambda_{\pm} = re^{i(\pi \pm \omega)}$, with $r = \sqrt{\lambda_c \lambda_v - C}$ and $\tan \omega = \sqrt{-4C - (\lambda_c - \lambda_v)^2}/(\lambda_c + \lambda_v)$, crosses the unit circle $(r = 1)$. For the latter case, the beat-to-beat oscillations of voltage and calcium are modulated with a period $2\pi/\omega$. Examination of the eigenvectors for $C < 0$ reveals that alternans are discordant when λ_- is real and $\lambda_c > \lambda_v$.

In Fig. 5 we plot the corresponding stability boundaries for positive and negative coupling in the (λ_c, λ_v) plane. We find that the boundaries of stability are remarkably isomorphic to that obtained by simulations of the ionic model in the (u, τ_f) plane of Fig. 3. Note that we have not used explicit functional forms for the map terms, but only exploited the basic structure of the map given by Eqs. (12)–(14), along with the important assumption that total calcium is constant from beat to beat. This agreement shows that the coupled dynamics of voltage and calcium can be understood qualitatively in terms of the basic features of the system.

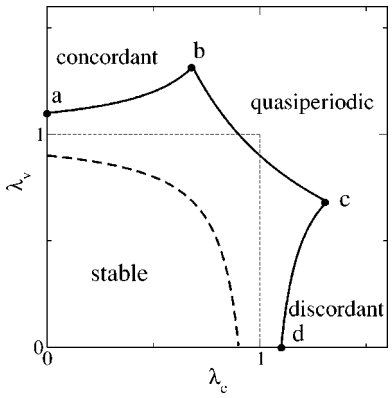

FIG. 5. Stability boundaries from the map analysis for positive coupling $C = 0.1$ with concordant alternans along the dashed line, and negative coupling $C = -0.1$ (solid line), with concordant alternans, discordant alternans, and quasiperiodicity along the segments a-b, c-d, and b-c, respectively.

V. CONCLUSION

The numerical study of both the ionic model and the map in the nonlinear regime reveals the existence of a rich dynamical behavior including higher order periodicities (3:3, 4:4, etc.) as well as transitions to chaos mediated by a period-doubling cascade or intermittency depending on the parameters. Moreover, this model naturally contains memory [21,23] due to the slow change of total calcium concentration over several beats. Both of these aspects will be discussed in more detail elsewhere.

In conclusion, we have outlined the essential three-dimensional parameter space that controls dynamic instability of membrane voltage coupled to calcium cycling, and we have presented a theoretical framework in which to interpret experiments beyond the limitations of the one-dimensional restitution relationship. The main axes of this parameter space are the degree of instability of the voltage and calcium systems, and the sign of the coupling between the two systems, which is an important parameter to emerge from this work. These results provide a starting point to explore the role of calcium cycling in the spatiotemporal dynamics of tissue scale phenomenon. For instance, it will be interesting to see how the more complex single cell dynamics presented here, influences the dynamics of spiral waves in tissue. Studies in this direction may shed light on the role of calcium cycling on cardiac rhythm disorders.

ACNOWLEDGMENT

This research was supported by NIH SCOR P50-HL52319.

[1] A. Karma, Chaos **4**, 461 (1994).
[2] A. Garfinkel *et al.*, Proc. Natl. Acad. Sci. U.S.A. **97**, 6061 (2000).
[3] M. Courtemanche, L. Glass, and J. P. Keener, Phys. Rev. Lett. **70**, 2182 (1993); B. Echebarria and A. Karma, *ibid.* **88**, 208101 (2002).
[4] J. B. Nolasco and R. W. Dahlen, J. Appl. Physiol. **25**, 191 (1968); M. R. Guevara *et al.*, in *Proceedings of the 11th Computers in Cardiology Conference* (IEEE Computer Society, Los Angeles, 1984), p. 167.
[5] G. M. Hall, S. Bahar, and D. J. Gauthier, Phys. Rev. Lett. **82**, 2995 (1999); G. M. Hall and D. J. Gauthier, *ibid.* **88**, 198102 (2002).
[6] J. J. Fox, E. Bodenschatz, and R. F. Gilmour, Jr., Phys. Rev. Lett. **89**, 138101 (2002).
[7] E. J. Pruvot *et al.*, Circ. Res. **94**, 1083 (2004).
[8] S. G. Dilly and M. J. Lab, J. Physiol. (London) **402**, 315 (1988).
[9] E. J. Chudin *et al.*, Biophys. J. **77**, 2930 (1999).
[10] M. E. Díaz, S. C. ONeill, and D. A. Eisner, Circ. Res. **94**, 650 (2004).
[11] Y. Shiferaw *et al.*, Biophys. J. **85**, 3666 (2003).
[12] J. J. Fox, J. L. McHarg, and R. F. Gilmour, Am. J. Physiol. **282**, H1534 (2002).
[13] C. H. Luo and Y. Rudy, Circ. Res. **74**, 1071 (1994).
[14] A. Fabiato, J. Gen. Physiol. **85**, 189 (1985).
[15] D. M. Bers, *Excitation-contraction Coupling and Cardiac Contractile Force* (Kluwer, Boston, 2001).
[16] M. L. Collier, A. P. Thomas, and J. R. Berlin, J. Physiol. (London) **516**, 117 (1999).
[17] W. G. Wier *et al.*, J. Physiol. (London) **474**, 463 (1994).
[18] T. R. Shannon, K. S. Ginsburg, and D. M. Bers, Biophys. J. **78**, 334 (2000).
[19] D. A. Eisner *et al.*, Circ. Res. **87**, 1087 (2000).
[20] D. S. Rubenstein and S. L. Lipsius, Circulation **91**, 201 (1995); M. L. Walker and D. S. Rosenbaum, Cardiovasc. Res. **57**, 599 (2003), and earlier references therein.
[21] R. F. Gilmour, N. F. Otani, and M. A. Watanabe, Am. J. Physiol. **272**, H1826 (1997); N. F. Otani and R. F. Gilmour, J. Theor. Biol. **187**, 409 (1997).
[22] L. Yin, H. Bien, and E. Entcheva (unpublished).
[23] M. A. Watanabe and M. L. Koller, Am. J. Physiol. **282**, H1534 (2002).